Department of APPLIED MATHEMATICS

Department of Mathematics
University of Bergen
5008 Bergen
Norway

ISSN 0084-778x

ELLAM-based Operator Splitting for Nonlinear Advection-Diffusion Equations

by

Helge K. Dahle

Report No. 98 June 1995

Universitetet i Bergen

UNIVERSITY OF BERGEN

Bergen, Norway

Department of Mathematics
University of Bergen
5008 Bergen
Norway

ISSN 0084-778x

ELLAM-based Operator Splitting for Nonlinear Advection-Diffusion Equations

by

Helge K. Dahle

Report No. 98

June 1995

ACKNOWLEDGMENTS

This research was supported in parts by VISTA, a research cooperation between the Norwegian Academy of Science and Letters and Den norske stats oljeselskap a.s (Statoil)

Abstract. Generalizations of Eulerian-Lagrangian localized adjoint methods (ELLAM) to nonlinear advection-diffusion equations in one space dimension are considered. Diffusion is modeled by standard piecewise linear finite elements at each new time-level. To model advection, consistent space-time extensions of elements and test functions are constructed by solving a first order conservation equation. First the basic algorithm is developed, then two approximations of time integrals are derived. The first approach is an Euler-backward-like scheme, the second is a Cranck-Nicolson-type scheme. Numerical experiments indicating optimal order convergence are presented.

Key words. Eulerian-Lagrangian localized adjoint methods (ELLAM), Godunov methods, nonlinear advection-diffusion equations.

1 Introduction

The numerical solution of advective-diffusive transport problems arise in many important applications in science and engineering. Such problems are difficult to discretize and conventional methods usually exhibit some combination of nonphysical oscillations or excessive numerical diffusion [12, 24]. Extra complications arise when the process is advection dominated or advection is nonlinear. It is therefor important to develop efficient methods that can treat different balances of nonlinear advection and diffusion in an accurate and consistent way within the same application.

The Eulerian-Lagrangian localized adjoint methods (ELLAM) [2, 13, 23], combines the ideas of the Eulerian-Lagrangian (EL) techniques, e.g. [10], and the localized adjoint methods (LAM), e.g. [1]. ELLAM schemes are based on constructing space-time elements and test functions aligned with the physical flow. This yield schemes that are optimal in space in some sense, and with small truncation errors in time. Thus, accurate and mass conservative schemes that treat general boundary conditions may be constructed.

ELLAM-schemes have been developed and analyzed for linear, transport-dominated flow problems both in one and multiple space dimensions [14, 22, 28, 29, 33, 34] and for systems of equations with nonlinear reaction terms [15, 16, 17, 18, 19, 20, 32, 35]. ELLAM schemes are also developed for the nonlinear Buckley-Leverett equation, based on a particular splitting of the flux-function [7].

In this paper a general approach to nonlinear transport problems are considered, based on combining a standard operator-splitting technique with a forward tracking ELLAM-scheme. Hence, by solving a first-order conservation equation in order to construct space-time elements, advection and diffusion are modeled in a consistent and accurate way. A 1'st order in time Euler-backward (EB) scheme and a 2'nd order Crank-Nicolson (CN) scheme are constructed based on this approach. The conservation equation is solved numerically by a Godunov-type method in this paper, but other methods may be considered.

The Godunov-Mixed Methods stated and analyzed in [8, 9] leads to a somewhat similar scheme as the EB-scheme derived in this paper. However, the Godunov-Mixed Methods approximate diffusion by a mixed finite element method in contrast to the standard element method used here.

In Section 2 the mathematical problem is stated and the basic splitting technique is derived. In Section 3 a suitable space-time test space is constructed, and in Section 4 two approximations of time integrals are considered. In Section 5 completely discretized schemes are derived based on using Godunov-type methods to solve the transport problem. Numerical experiments are outlined in sections 5 and 6 and some error estimates are verified. Furthermore, qualitative properties of the schemes are discussed. Finally, conclusions are given in Section 6.

2 Operator splitting

Let $u(x,t)$ satisfy the initial-value problem

$$\begin{aligned} \mathcal{P}u = \frac{\partial u}{\partial t} + \frac{\partial}{\partial x}\left\{f(u) - D\frac{\partial u}{\partial x}\right\} = 0, &\quad (x,t) \in \mathbf{R}^2_+, \\ u(x,0) = u_0(x), &\quad -\infty < x < \infty. \end{aligned} \tag{1}$$

Here $\mathcal{P}$ is a parabolic operator, f is the advective flux, D is the diffusion coefficient (assumed for simplicity to be constant) and u_0 is a known function of x.

Let $U(x,t)$ approximate the analytic solution $u(x,t)$ of (1). Define $S_h \subset H^1_0(\mathbf{R})$ to be a finite-element approximation space on a partitioning $\{x_i\}$ of the real-axis. For convenience, choose $x_i = i\Delta x$, $i = 0, \pm1, \pm2, ...$ The problem is to determine $U^{n+1}(x) = U(x, t^{n+1}) \in S_h$ at discrete time-levels $t^{n+1} = (n+1)\Delta t$, $n = 0, 1, ..., N$, with $U^0(x)$ being a suitable approximation of $u_0(x)$.

Let $\Omega^{n+1} = (-\infty, \infty) \times [t^n, t^{n+1}]$ denote a space-time strip in $\mathbf{R}^2_+$. Replace u by U in (1), multiply the equation by a test function $w(x,t) \in H^1_0(\Omega^{n+1})$ and integrate-by-parts over Ω^{n+1}. Since $w(-\infty, t) = w(\infty, t) = 0$, the following local weak form of equation (1) is obtained:

$$\begin{aligned} &\int_{t^n}^{t^{n+1}} \int_{-\infty}^{\infty} \left\{ U w_t + \left(f(U) - D\frac{\partial U}{\partial x} \right) w_x \right\} dx dt \\ &= \int_{-\infty}^{\infty} U^{n+1} w^{n+1} dx - \int_{-\infty}^{\infty} U^n w^n dx \end{aligned} \tag{2}$$

where (2) must be satisfied for every admissible test function $w(x,t)$.

Next, split $U(x,t)$ into two parts

$$U(x,t) = U_0(x,t) + U_1(x,t), \tag{3}$$

where U_0 is a solution of a related initial-value problem:

$$\begin{aligned} \mathcal{P}_0 U_0 = 0, &\quad -\infty < x < \infty, \quad t^n < t \leq t^{n+1}, \\ U_0(x, t^n) = U^n(x), &\quad -\infty < x < \infty. \end{aligned} \tag{4}$$

The operator $\mathcal{P}_0$ approximates $\mathcal{P}$ and may be chosen in various ways depending on the particular problem considered. For transport dominated processes a natural choice is:

$$\mathcal{P}_0 U_0 = \frac{\partial U_0}{\partial t} + \frac{\partial}{\partial x}\{f(U_0)\}. \tag{5}$$

It is well known that nonlinear flux-functions may generate solutions that possess shocks. Weak solutions of (3), (5) on Ω^{n+1} are defined by:

$$\begin{aligned}&\int_{t^n}^{t^{n+1}}\int_{-\infty}^{\infty}\{U_0 w_t + f(U_0)w_x\}\,dxdt\\&=\int_{-\infty}^{\infty}U_0^{n+1}w^{n+1}dx-\int_{-\infty}^{\infty}U^n w^n dx,\end{aligned}\qquad \forall w(x,t)\in C_0^1(\Omega^{n+1}). \tag{6}$$

A physical solution of (6) is uniquely determined by the entropy condition [26]:

$$\frac{f(u)-f(u_l)}{u-u_l}\geq s\geq\frac{f(u)-f(u_r)}{u-u_r}, \tag{7}$$

for all u between u_l and u_r. Here, u_l and u_r denote the left- and right-hand-side values of a discontinuity propagating in time (shock curve) with shock-speed s given by the Rankine-Hugoniot jump condition:

$$s=\frac{f(u_l)-f(u_r)}{u_l-u_r}. \tag{8}$$

As a consequence of (7), *no characteristic drawn in the direction of decreasing t intersects a shock curve* [25]. This observation is important for the construction of test functions.

Assume that an (approximate) entropy solution U_0 of (6) exists. Expand the flux function around U_0 by:

$$f(U)=f(U_0)+f'(U_0)U_1+\frac{1}{2}f''(\hat{U})U_1^2, \tag{9}$$

where $\hat{U}$ is between U_0 and U. Insert (9) into (2) and get:

$$\begin{aligned}&\int_{t^n}^{t^{n+1}}\int_{-\infty}^{\infty}\left(U_0w_t+f(U_0)w_x-D\frac{\partial U}{\partial x}\frac{\partial w}{\partial x}\right)dxdt\\&+\int_{t^n}^{t^{n+1}}\int_{-\infty}^{\infty}U_1\left(w_t+f'(U_0)w_x+\frac{1}{2}f''(\hat{U})U_1^2w_x\right)dxdt\\&=\int_{-\infty}^{\infty}U^{n+1}w^{n+1}dx-\int_{-\infty}^{\infty}U^nw^ndx.\end{aligned} \tag{10}$$

Let

$$\mathcal{P}_0^*w=-w_t-f'(U_0)w_x \tag{11}$$

denote the "adjoint" of $\mathcal{P}_0$. This coincide with the usual definition of an adjoint when f is linear. Equation (11) is motivated by the fact that $f'(U_0)$ approximates the particle speed, except for possible lines of discontinuity (shock curves) of U_0. Hence, $\mathcal{P}_0^*$ as defined by (11), reflects the Lagrangian nature of the problem.

Combine (10), (11) with (6), neglect the second-order term in U_1 and obtain:

$$\begin{aligned}\int_{-\infty}^{\infty}U^{n+1}w^{n+1}dx+\int_{t^n}^{t^{n+1}}\int_{-\infty}^{\infty}D\frac{\partial U}{\partial x}\frac{\partial w}{\partial x}dxdt&=\int_{-\infty}^{\infty}U_0^{n+1}w^{n+1}dx\\&+\int_{t^n}^{t^{n+1}}\int_{-\infty}^{\infty}U_1\mathcal{P}_0^*w\,dxdt,\end{aligned} \tag{12}$$

for every admissible test function $w(x,t)\in C_0^1(\Omega^{n+1})$. Note that the only approximation used in deriving (12) from (2) is the linearization given by neglecting the second order term in (9). In the linear case, $f''\equiv 0$, this becomes exact.

3 Construction of a Test Space

Let $T_h \subset C_0^1(\Omega^{n+1})$ denote a discrete test space. Motivated by ELLAM concepts, choose space-time test functions that makes $\mathcal{P}_0^*$ vanish or as small as possible. To achieve this, let $S_h = span\{\theta_i,\ i = 0, \pm 1, ...\}$, then a test space $T_h = span\{w_i,\ i = 0, \pm 1, ...\}$ is determined by

$$\begin{aligned} \mathcal{P}_0^* w_i = -\frac{\partial w_i}{\partial t} - f'(U_0)\frac{\partial w_i}{\partial x} = 0, &\quad \infty < x < \infty, \quad t^n \le t < t^{n+1}, \\ w_i(x, t^{n+1}) = \theta_i(x), &\quad -\infty < x < \infty. \end{aligned} \tag{13}$$

This is a *linear* advection equation, to be solved *backward* in time. Characteristics associated with the operators $\mathcal{P}_0$, $\mathcal{P}_0^*$ as defined by (5), (11), are given by:

$$\frac{dx}{d\tau} = f'(U_0), \quad \frac{dt}{d\tau} = 1. \tag{14}$$

If U_0 is smooth, then U_0 and w_i are constant along the characteristics, thus given by straight lines:

$$x^*(x, t; \tau) = x - f'(U_0)(t - \tau), \quad t^n \le \tau \le t^{n+1}, \tag{15}$$

Hence, for characteristics not intersecting lines of discontinuity

$$U_0(x,t) = U^n(x^*(x,t;t^n)) \text{ and } w_i(x,t) = \theta_i(x^*(x,t;t^{n+1})), \quad t^n \le t \le t^{n+1}.$$

Suppose U_0 possesses a shock propagating along the curve

$$x_s = x_s(\tau), \quad t^n \le t_s \le \tau \le t^{n+1},$$

t_s being the time when the shock first appears. Let $U_{0_l}^{n+1}$ and $U_{0_r}^{n+1}$ be the left- and right-hand-side values of U_0 at $(x_s(t^{n+1}), t^{n+1})$. Consequently, two characteristics meet at $(x_s(t^{n+1}), t^{n+1})$:

$$\begin{aligned} x_l^*(t) &= x_s(t^{n+1}) - f'(U_{0_l}^{n+1})(t^{n+1} - t), \\ x_r^*(t) &= x_s(t^{n+1}) - f'(U_{0_r}^{n+1})(t^{n+1} - t). \end{aligned}$$

Let R_s denote the shock region

$$R_s = \left\{(x,t) \mid x_l^*(t) \le x \le x_r^*(t),\ t^n \le t \le t^{n+1}\right\}, \tag{16}$$

see Figure 1(a). Since no characteristics tracked backward from time-level t^{n+1} intersect R_s, test functions on R_s are arbitrarily prescribed by the values along the shock curve. The simplest possible continuous space-time test function satisfying (13) everywhere, is therefor defined by taking the constant value $\theta_i(x_s(t^{n+1}))$ on R_s. On the other hand, by (7), characteristics can not diverge from a physical shock. In this way the entropy condition enters the construction to ensure $T_h \subset C_0^1$. The only possible case when characteristics may diverge from a discontinuity, is a rarefaction wave issuing from an initial discontinuity say at $(x_s, 0)$. Such points of exception may create some numerical difficulties, see below.

To summarize the construction: Each space-time strip Ω^{n+1} is divided into regions where U_0 is smooth and possibly a finite number of shock regions R_s. Space-time test functions are defined by

$$w_i(x,t) = \begin{cases} \theta_i(x^*(x,t;t^{n+1})), & (x,t) \in \Omega^{n+1} \backslash R_s, \\ \theta_i(x_s(t^{n+1})) & (x,t) \in R_s. \end{cases} \tag{17}$$

By choice of $\mathcal{P}_0^*$, these test functions also reflects the Lagrangian nature of the problem. Space-time elements Ω_i^{n+1} are defined by tracking characteristics $x^*(t)$ backward from nodes (x_{i-1}, t^{n+1}) and (x_i, t^{n+1}), see Figure 1(a). By convention, track $x_r^*(t)$ if a node coincide with $x_s(t^{n+1})$. Hence, if a discontinuity appears at $x_s(t^{n+1})$, $x_{i-1} < x_s(t^{n+1}) \leq x_i$, then $R_s \subset \Omega_i^{n+1}$. With θ_i being the usual hat functions, a test function $w_i(x,t)$ with support on R_s is depicted in Figure 1(b). Figure 2 shows elements used in a computation.

Remark: By the definition of $\mathcal{P}_0$ we may generally assume U_1 to be small in absolute value which allows us to neglect the second order term in U_1 in equation (12). This is not the case when U_0 develops a shock within a time step, since U will always remain smooth ($t > 0$). However, by the construction of test functions, the second-order term in U_1 will in fact vanish on R_s since this term is multiplied by w_x and $w_x \equiv 0$ on R_s.

4 Approximations of time integral

Combining(12), (13) and (17), successive approximations to (1) are given by the problems; Find $U^{n+1} \in S_h$, $n = 0, 1, ..., N$, such that:

$$\int_{-\infty}^{\infty} U^{n+1}\theta_i dx + \int_{t^n}^{t^{n+1}} \int_{-\infty}^{\infty} D\frac{\partial U}{\partial x}\frac{\partial w_i}{\partial x} dxdt = \int_{-\infty}^{\infty} U_0^{n+1}\theta_i dx, \quad i = 0, \pm 1, \dots . \tag{18}$$

To approximate the time integral, assume for simplicity that U_0 possesses only one shock propagating along the curve $x = x_s(t)$, such that $x_l^*(t) \leq x_s(t) \leq x_r^*(t)$. Then, by (16), (17):

$$\int_{t^n}^{t^{n+1}} \int_{-\infty}^{\infty} D\frac{\partial U}{\partial x}\frac{\partial w_i}{\partial x} dxdt = \left(\int_{t^n}^{t^{n+1}} \int_{-\infty}^{x_l^*(t)} + \int_{t^n}^{t^{n+1}} \int_{x_r^*(t)}^{\infty} \right) D\frac{\partial U}{\partial x}\frac{\partial w_i}{\partial x} dxdt. \tag{19}$$

By (14), (15), Lagrangian coordinates are given by:

$$t(\xi,\tau) = \tau, \quad x(\xi,\tau) = \xi - f'(U_0^{n+1}(\xi))(t^{n+1} - \tau). \tag{20}$$

The Jacobian of this map reduces to:

$$\frac{\partial(x,t)}{\partial(\xi,\tau)} = \frac{\partial x}{\partial \xi}.$$

Hence, (19) transform as:

$$\int_{t^n}^{t^{n+1}} \int_{-\infty}^{\infty} D\frac{\partial U}{\partial x}\frac{\partial w_i}{\partial x} dxdt = \left(\int_{-\infty}^{x_s(t^{n+1})} \int_{t^n}^{t^{n+1}} + \int_{x_s(t^{n+1})}^{\infty} \int_{t^n}^{t^{n+1}} \right) D\frac{\partial U}{\partial x}\frac{\partial w_i}{\partial x}\frac{\partial x}{\partial \xi} d\tau d\xi, \tag{21}$$

since (20) maps $\xi = \textit{constant}$ onto characteristics through (ξ, t^{n+1}). We consider two approximations of (21):

(i) Euler-backward (EB): Approximate the integrand in (21) by the value at the head of the characteristic:

$$\left(D\frac{\partial U}{\partial x}\frac{\partial w_i}{\partial x}\frac{\partial x}{\partial \xi} \right)(\xi,\tau) \approx D\frac{\partial U^{n+1}}{\partial x}\frac{\partial \theta_i}{\partial x}. \tag{22}$$

Combine (21) and (22) with (18) and obtain:

$$\int_{-\infty}^{\infty} U^{n+1}\theta_i dx + \Delta t \int_{-\infty}^{\infty} D\frac{\partial U^{n+1}}{\partial x}\frac{\partial \theta_i}{\partial x} dx dt = \int_{-\infty}^{\infty} U_0^{n+1}\theta_i dx, \quad i = 0, \pm 1, \dots . \tag{23}$$

Note that equations (23) are completely symmetric and does not require explicit evaluations of $w_i(x,t)$, $t < t^{n+1}$.

(ii) Crank-Nicolson (CN): Replace the integrand in (21) by the average of the values at the foot and the head of the characteristics:

$$\left(D\frac{\partial U}{\partial x}\frac{\partial w_i}{\partial x}\frac{\partial x}{\partial \xi}\right)(\xi,\tau) \approx \frac{1}{2}\left(D\frac{\partial U^{n+1}}{\partial x}\frac{\partial \theta_i}{\partial x} + D\frac{\partial U^{n}}{\partial x}\frac{\partial w_i^n}{\partial x}\frac{\partial x}{\partial \xi}^{n}\right). \tag{24}$$

Combine (21) and (24) with (18), transform back to Eulerian coordinates and get:

$$\begin{aligned} &\int_{-\infty}^{\infty} U^{n+1}\theta_i dx + \frac{\Delta t}{2}\int_{-\infty}^{\infty} D\frac{\partial U^{n+1}}{\partial x}\frac{\partial \theta_i}{\partial x} dx \\ &= \int_{-\infty}^{\infty} U_0^{n+1}\theta_i dx \ - \frac{\Delta t}{2}\int_{-\infty}^{\infty} D\frac{\partial U^{n}}{\partial x}\frac{\partial w_i^n}{\partial x} dx, \end{aligned} \qquad i = 0, \pm 1, \dots, \tag{25}$$

where we have used that $\partial w_i^n/\partial x \equiv 0$, $x \in [x_l^*(t^n), x_r^*(t^n)]$. Again, (25) is completely symmetric. In computations w_i^n is approximated by piecewise linear functions on the partitioning $\{x_i^*\}$ of the x-axis as suggested in Figure 1(b).

Although Crank-Nicolson is unconditionally stable for linear problems, unwanted finite oscillations can occur in the presence of discontinuities or sharp gradients, due to the partly explicit treatment of diffusion [30]. Because of this one might expect the CN-scheme to perform poorly in the presence of fronts generated by the nonlinearity in f. This is generally not true since the explicit part of such fronts are smeared out or removed by the definition of test functions. On the other hand, oscillations will appear when a rarefaction wave is computed from an initial discontinuity by the CN-scheme. Such oscillations may be filtered away, e.g. by taking an EB-step initially .

5 Numerical investigations

In the following, let S_h be a standard piecewise linear trial space with nodes at $\{x_i\}$. Analytical expressions for U_0^{n+1} are generally not feasible. However, U_0^{n+1} may be computed independently by explicit methods, e.g. higher-order Godunov schemes. To simplify the exposition, assume we have chosen to use Godunov's method to solve (4), (5). Let $\Delta x_g = \Delta x/N_h$ and $\Delta t_g = \Delta t/N_t$ be the space- and time-step used to approximate U_0^{n+1}. N_h and N_t are integers chosen so that the CFL-condition is maintained. Godunov's method computes approximations $\tilde{U}_0$ to U_0, at time levels $t^{n+\frac{j}{N_t}}$, $j = 1, 2, \dots, N_t$, represented by:

$$\tilde{U}_0^{n+\frac{j}{N_t}}(x) = \sum_{i=-\infty}^{\infty} U_{0,i}^{j}\chi_i(x), \quad j = 1, 2, \dots, N_t, \tag{26}$$

where $\chi_i(x)$ is the characteristic function:

$$\chi_i(x) = \begin{cases} 1 & (i-1/2)h_g \le x \le (i+1/2)\Delta x_g, \\ 0 & \text{otherwise.} \end{cases}$$

The initial data corresponding to $j = 0$ in (26) is determined from $U^n(x)$ by averaging:

$$U_{0_i}^0 = \frac{1}{\Delta x_g} \int_{(i-1/2)\Delta x_g}^{(i+1/2)\Delta x_g} U^n(x)dx, \quad i = 0, \pm 1, ...$$

From the representation (26), an approximate right-hand-side of (18) is given by:

$$(U_0^{n+1}, \theta_i) \approx (\tilde{U}_0^{n+1}, \theta_i), \tag{27}$$

where the last inner product is computed by exact integration. Since Godunov's method is only first order, errors will accumulate unless $\Delta t_g \ll \Delta t$. In computations we have used the slope-limiter method given in [21]. This extension is straight forward, and is obtained by replacing (26) by:

$$\tilde{U}_0^{n+\frac{j}{N_t}}(x) = \sum_{i=-\infty}^{\infty} \left(U_{0_i}^j + s_i^j(x - i\Delta x_g) \right) \chi_i(x), \quad j = 1, 2, ..., N_t, \tag{28}$$

where s_i^j is the slope limiter. It is well known that Godunov-type methods are diffusive and does not track shocks/fronts explicitly like for example front tracking methods. Possible shock values $(\tilde{x}_s^{n+1}, \tilde{U}_{0_l}^{n+1}, \tilde{U}_{0_r}^{n+1})$ to be used by the CN-scheme, are here estimated by direct inspection of data $\{\tilde{U}_{0_i}^{N_t}\}$. There is no unique way of doing this and details are omitted here.

Consider the linear problem defined by $f(u) = Vu$, where V is a constant particle speed. In Lagrangian coordinates (1) transforms to the standard heat equation and (18) reduces to a variational form of the heat equation. Using that

$$U_0^{n+1}(x) = U^n(x - V\Delta t) \text{ and } w_i^n(x) = \theta_i(x + V\Delta t)$$

the integrals in (23) and (25) can be determined exactly. Hence, by standard arguments, see for example [31], optimal order error estimates for the EB- and CN-scheme in the L_2-norm are respectively:

$$\left\| U_{\text{EB}}^{N+1} - u(t^{N+1}) \right\|_2 \le C_1(\Delta t + \Delta x^2) \tag{29}$$

and

$$\left\| U_{\text{CN}}^{N+1} - u(t^{N+1}) \right\|_2 \le C_2(\Delta t^2 + \Delta x^2), \tag{30}$$

where C_1 and C_2 are constants. Note that time-truncation errors should be evaluated along characteristics.

The main new feature introduced by nonlinearity, is existence of self-sharpening fronts. The simplest possible test problem involving a self sharpening front is the following initial value problem for Burgers' equation:

$$\begin{aligned} u_t + uu_x &= Du_{xx}, \qquad (x,t) \in \mathbf{R}_+^2, \\ u(x,0) &= \begin{cases} 1 & -\infty < x \le 0, \\ 1 - 2x & 0 \le x \le 1/2, \\ 0 & 1/2 \le x \le \infty. \end{cases} \end{aligned} \tag{31}$$

For large times the solution of (31) approaches a quasi-steady state, given by [27]:

$$u(x,t) = \frac{1}{2} - \frac{1}{2}\tanh\left(\frac{1}{4D}\left[x - \frac{1}{2}t - \frac{1}{2}\right]\right). \tag{32}$$

The main sources of errors not accounted for in the linear estimates (29), (30), are the linearization (9), (10) and the approximation of the L_2-projection of U_0 by (27). We are not concerned about the approximation (27), and eliminate this by making $\Delta x_g \ll \Delta x$ and $\Delta t_g \ll \Delta t$. Furthermore, the computations are truncated in space by assuming that the solution satisfy:

$$u(x,t) = \begin{cases} 1., & x < -0.5, \\ 0., & x > 3. \end{cases} \tag{33}$$

By choosing $0 \leq t \leq 3.2$ and $D = 0.05$, the error due to this truncation seems to be (mostly) negligible. Note also that any other choice of D may be transformed back to this example by rescaling the x- and t-axis. In Figure 3 the solution is computed using the CN-scheme and compared with the asymptotic solution (32). In Figures 5 and 6 the logarithm of the L_2-error:

$$error = \sqrt{\int_{-0.5}^{3.0} (U^{N+1} - u(x,t^{N+1})^2)\,dx}$$

is computed as a function of $\log \Delta t$ with $\Delta x \ll 1$ fixed (Figure 5), and $\log \Delta x$ with $\Delta t \ll 1$ fixed (Figure 6). Here, $t^{N+1} = 2.4$, U^{N+1} is computed by the CN- and the EB-scheme, and $u(x,t)$ is given by (32). Assume that

$$error_{\mathrm{EB}} \sim C_1(\Delta t^{p_{\mathrm{EB}}} + \Delta x^{k_{\mathrm{EB}}}) \tag{34}$$

and

$$error_{\mathrm{CN}} \sim C_2(\Delta t^{p_{\mathrm{CN}}} + \Delta x^{k_{\mathrm{CN}}}), \tag{35}$$

where C_1 and C_2 are constants. Using linear regression to determine a best linear fit to the data in Figures 5 and 6, gives $p_{\mathrm{EB}} = 0.98$, $k_{\mathrm{EB}} = 2.02$, $p_{\mathrm{CN}} = 1.82$ (omitting the two first data points, see next section) and $k_{\mathrm{CN}} = 2.06$. The loss of convergence rate for the CN-scheme when $\Delta t \to 0$, is caused by erroneous fluxes at the boundaries due to the truncation (33). By leaving out the two data points given by the smallest Δt (as well as the two largest) gives $p_{\mathrm{CN}} = 2.06$.

6 Large time-step behavior

In the previous section we investigated asymptotical behavior for small Δt, Δx. Practical problems are ofte characterized by slow time scales when viewed in Lagrangian coordinates. It is therefor important to investigate large time step performance when this is consistent with the physical problem studied. In fact, since test functions (17) are constructed to reflect the Lagrangian nature of the problem, we expect long, stable and accurate time steps to be feasible.

Assume that the solution posses a traveling front. Split f into two parts

$$f(u) = \bar{f}(u;t) + d(u;t), \tag{36}$$

such that $\bar{f}'$ represents the actual particle speed. The parameter t indicates that the splitting generally is time dependent. In the limit $D \to 0$, $\bar{f}$ is given by:

$$\bar{f} = \begin{cases} f(u), & \max(u_l, u_r) < u, \\ su, & \min(u_l, u_r) < u < \max(u_l, u_r), \\ f(u), & u < \min(u_l, u_r), \end{cases} \tag{37}$$

where s is the shock speed (8) and u_l, u_r are the right- and left-hand-side values respectively of the discontinuity. The width of the front is $O(D/|d'|)$, where $|d'| \sim \max_u |\partial d/\partial u|$, since the diffusive flux is asymptotically balanced by the residual advective flux d. Suppose this front can be resolved in the trial-space S_h. The front-width of the approximate solution obtained from the EB-scheme is easily seen to be of $O((D\Delta t)^{\frac{1}{2}})$ for reasonable large Δt, since U_0 at most can sharpen to a discontinuity in each time step. Consequently, if U_0 has sharpened to a maximum shock in time Δt, then a too wide front-width is computed unless $\Delta t \sim D/(|d'|)^2$. Introducing the Courant number $Cu = \Delta t|d'|/\Delta x$ and the mesh Péclet number $Pe = \Delta x|d'|/D$, both relative the residual advective flux d, we see that the approximated front becomes to wide, unless Cu is chosen so that

$$Cu \sim Pe^{-1}, \tag{38}$$

or less. Note that (38) is not a stability bound, but merely a measure of an optimal choice of time step in terms of obtaining correct balance between advection (sharpening) and diffusion. This bound is of course only of importance in the presence of fronts, since $d(u) \equiv 0$ otherwise.

The bound (38) can be somewhat reduced by taking the shock region R_s into account, as done by the CN-scheme. In fact, by a similar heuristic argument as above, the following bound is obtained for the CN-scheme

$$Cu < 2Pe^{-1}, \tag{39}$$

since diffusion is effectively halfed in the front region by the CN-scheme. However, this argument also shows that we at most can expect first-order convergence in time for large time steps. This may explain the "bend" in the CN-curve in Figure 5. On the other hand, as shown in Figure 4 and Figure 5, the CN-scheme obviously perform better than the EB-scheme even for large Δt.

In many cases approximate splittings (36), (37) are known and may be utilized [3, 4, 5, 6, 11]. For example, the solution of problem (31) approaches a traveling quasi-steady state leading to $\bar{f}(u) = u/2$ after a certain time $t_s \sim 1/2$. In such cases it may be natural to choose

$$\mathcal{P}_0 U_0 = \frac{\partial U_0}{\partial t} + \frac{\partial}{\partial x}(\bar{f}(U_0))$$

and group the residual advective term together with diffusion to obtain a more accurate balance between diffusion and advective sharpening. This lead to nonsymmetry, and care must be taken to construct test spaces that yield stable and not too diffusive schemes, see for example [3, 5].

7 Conclusions

The aim of the ELLAM methodology is to systematically discretize advection-diffusion problems with general boundary conditions in an accurate, mass-conservative, oscillation-free manner. Previous papers have carried this out successfully for problems with linear transport terms, and to some extent, for nonlinear transport. The present work is the first to combine ELLAM with Godunov-type methods to handle nonlinear advection in a general way.

One of the interests of this work has been to see if a second-order in time ELLAM scheme is feasible in the presence of fronts generated by nonlinearity. The conclusion based on the experiments performed here is affirmative. However, the implementation is fairly complicated and for more general problems $O(\Delta t)$-approximations may easily enter the computations, e.g. at the boundaries.

The main result from this work is the derivation of an operator-splitting technique for a nonlinear conservation equation within the ELLAM-framework. Since the choice of splitting in some sense is arbitrary (determined by physical considerations), different solution strategies for the advection part may be relevant. In this paper, Godunov schemes are choosen because of their generality and robustness. We also note that the operator splitting choosen here leads to completely symmetrized equations, which is numerically desirable.

The problem of determining optimal space- and time-steps for the computation of the approximate solution $\tilde{U}_0$ of the hyperbolic problem, has not been investigated. The loss of accuracy from taking the L_2-projection of this approximation onto the trial space is difficult to analyze, since the errors in the final approximate solution and the errors in $\tilde{U}_0$ are measured in different norms.

Work is now in progress to extend the proposed scheme (1'st-order in time) to the Buckley-Leverett equation, whith different boundary conditions being considered. We are also in the process of extending the scheme to three-phase flow. The results so far are promising.

References

[1] M.A. Celia, I. Herrera, and E.T. Bouloutas, *Adjoint Petrov-Galerkin methods for multidimensional flow problems*, Proceedings of the Seventh International Conference on Finite Element Methods in Flow Problems, Huntsville, AL, April 3-7, 1989, pp. 953-958.

[2] M.A. Celia, T.F. Russell, I. Herrera and R.E. Ewing, *An Eulerian-Lagrangian localized adjoint method for the advection-diffusion equation*, Adv. Water Resources, 1990, Vol. 13, No.4, 187-206.

[3] H.K. Dahle, M.S. Espedal and R.E. Ewing, *Characteristic Petrov-Galerkin subdomain methods for convection diffusion problems*, M.F. Wheeler (ed.), Mathematics in Oil Recovery, IMA Volumes in Mathematics and its Applications, Vol.11, 1988.

[4] H.K. Dahle and M.S. Espedal, *Local refinement techniques for two-phase immiscible flow in porous media*, Proceedings of the Seventh International Conference on Finite Element Methods in Flow Problems, Huntsville, AL, April 3-7, 1989, pp. 953-958.

[5] H.K. Dahle, M.S. Espedal, R.E. Ewing and O. Sævareid, *Characteristic Adaptive Subdomain Methods for Reservoir Flow Problems*, Numerical Methods for Partial Differential Equations, 6 (1990), 279-309.

[6] H.K. Dahle, M.S. Espedal and O. Sævareid, *Characteristic, Local Gridrefinement Techniques for Reservoir Flow Problems*, Int. J. Num. Meth.Eng., Vol. 33, 1992.

[7] H.K. Dahle, R.E. Ewing, T.F. Russell, *Eulerian-Lagrangian Localized Adjoint Methods for a Nonlinear Advection-Diffusion Equation*, Submitted to Comp. Meth. in Appl. Mech. and Eng.

[8] C.N. Dawson, *Godunov mixed methods for advective flow problems in one space dimension*, SIAM J. Numer. Anal., 28 (1991), pp. 1282-1309.

[9] C.N. Dawson, *Godunov mixed methods for advection-diffusion equations in multidimensions*, SIAM J. Numer. Anal., 30 (1993), pp. 1315-1332.

[10] J. Douglas, Jr. and T.F. Russell, *Numerical methods for convection-dominated diffusion problems based on combining the method of characteristics with finite element or finite difference procedures*, SIAM J. Numer. Anal., 19 (1982), 871-885

[11] M.S. Espedal and R.E. Ewing, *Characteristic Petrov-Galerkin subdomain methods for two-phase immiscible flow*, Comp. Meth. in Appl. Mech. and Eng., 64 (1987), 113-135.

[12] R.E. Ewing, ed., *The Mathematics of Reservoir Simulation*, Frontiers in Applied Mathematics 1, SIAM, Philadelphia, 1983.

[13] R.E. Ewing, *Operator splitting and Eulerian-Lagrangian localized adjoint methods for multiphase flow*, J. Whiteman (ed.), The Mathematics of Finite Elements and Applications VII MAFELAP 1990, Academic Press, San Diego, 1991, pp. 215-232.

[14] R.E. Ewing, H. Wang, *Eulerian-Lagrangian localized adjoint methods for linear advection equations*, Computational Mechanics '91, Springer International, 1991, 245-250.

[15] R.E. Ewing and H. Wang, *Eulerian-Lagrangian localized adjoint methods for reactive transport in groundwater*, to appear in IMA Volume in Mathematics and Its Applications, Wheeler *et al.*, (eds.), Springer Verlag, Berlin.

[16] R.E. Ewing and H. Wang, *An Eulerian-Lagrangian localized adjoint method for variable-coefficient advection-reaction problems*, Advances in Hydro-Science and Engineering, Vol I (B), 1993, 2010–2015.

[17] R.E. Ewing and H. Wang, *Eulerian-Lagrangian localized adjoint methods for linear advection or advection-reaction equations and their convergence analysis*, Computational Mechanics, Vol. 12, Num. 1/2, (1993), 97–121.

[18] R.E. Ewing and H. Wang, *Eulerian-Lagrangian localized adjoint methods for variable-coefficient advective-diffusive-reactive equations in groundwater contaminant transport*, Advances in Optimization and Numerical Analysis, Mathematics and Its Applications, Vol 275. Kluwer Academic Publishers, Dordrecht, Netherlands, (1994), 185–205.

[19] R.E. Ewing, H. Wang and R.C Sharpley, *Eulerian-Lagrangian localized adjoint methods for transport of nuclear-waste contamination in porous media*, Computational Methods in Water Resources X. Vol. I, Water Science and Technology Library, Vol 12. Kluwer Academic Publishers, Dordrecht, Netherlands, (1994), 241–248.

[20] R.E. Ewing and H. Wang, *An optimal-order error estimate to Eulerian-Lagrangian localized adjoint method for variable-coefficient advection-reaction problems*, to appear in SIAM J. Numer. Anal., Vol. 33, No. 2.

[21] J.B. Goodman, R.J. LeVeque, *A geometric approach to high resolution TVD schemes*, SIAM J. Numer. Anal., 25 (1988), pp. 268-284.

[22] R.W. Healy and T.F. Russell, *A finite-volume Eulerian-Lagrangian localized adjoint method for solution of the advection-dispersion equation*, Water Resources Research, to appear.

[23] I. Herrera and R.E. Ewing, M.A. Celia and T.F. Russell, *Eulerian-Lagrangian localized adjoint methods: The theoretical framework*, To appear in SIAM J. Numer. Anal.

[24] C. Johnson, *Numerical Solution of Partial Differential Equations by the Finite Element Method*, Cambridge University Press, 1990.

[25] P.D. Lax, *Hyperbolic Systems of Conservation Laws and the Mathematical Theory of Shock Waves*, SIAM Regional Conference Series in Applied Mathematics, 11, 1972.

[26] R.J. LeVeque, *Numerical Methods for Conservation Laws*, Birkhäuser, 1990.

[27] T.F. Russell, *Galerkin time stepping along characteristics for Burgers' equation*, R. Stepleman et al. (eds.), Scientific Computing, IMACS, North-Holland, 1983, pp. 183-192.

[28] T.F. Russell, *Eulerian-Lagrangian localized adjoint methods for advection-dominated problems*, D.F. Griffiths and G.A. Watson (eds.), Numerical Analysis 1989, Pitman Research Notes in Mathematics Series, Vol. 228, Longman Scientific & Technical, Harlow, U.K., 1990, pp. 206-228.

[29] T.F. Russell and R.V. Trujillo, *Eulerian-Lagrangian localized adjoint methods with variable coefficients in multiple dimensions*, G. Gambolati et al. (eds.), Computational Methods In Surface Hydrology, Proceedings of the Eighth International Conference on Computational Methods in Water Resources, Computational Mechanics Publications, Southampton, 1990, pp. 357-363.

[30] G.D. Smith, *Numerical Solution of Partial Differential Equations: Finite Difference Methods*, Oxford University press, 1985.

[31] V. Thomée, *Galerkin Finite Element Methods for Parabolic Problems*, Lecture Notes in Mathematics, 1054, Springer-Verlag, 1984.

[32] J.E. Våg, H. Wang and H.K. Dahle, *Eulerian-Lagrangian localized adjoint methods for systems of nonlinear advective-diffusive-reactive equations*, in preparation.

[33] H. Wang, R.E. Ewing and T.F. Russell, *Eulerian-Lagrangian localized adjoint methods for convection-diffusion equations and their convergence analysis*, IMA J. Numer. Anal., submitted.

[34] H. Wang, R.E. Ewing and T.F. Russell, *ELLAM for variable-coefficient convection-diffusion problems arising in groundwater applications*, Computational Methods in Water Resources IX. Vol. I: Numerical Methods in Water Resources, Computational Mechanics Publications and Elsevier Applied Science, London and New York, 1992, 25-31.

[35] H. Wang, R.E. Ewing and M.A. Celia, *Eulerian-Lagrangian localized adjoint method for reactive transport with biodegradation*, Numerical Methods for PDE's, submitted.

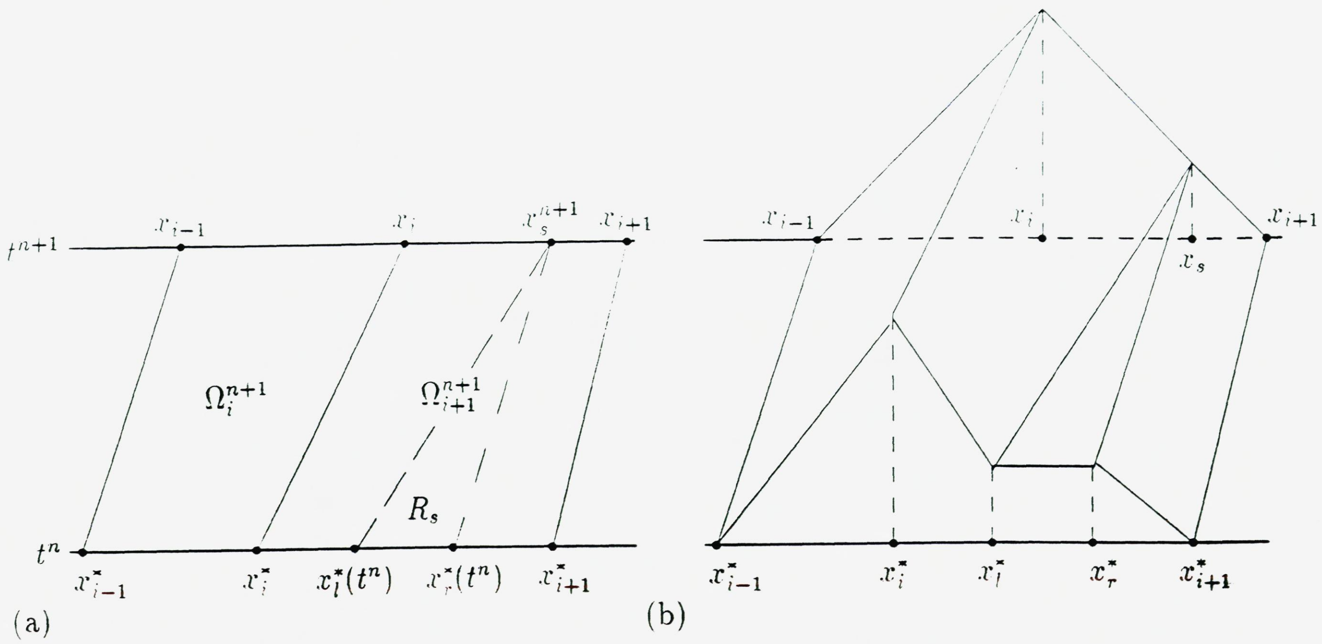

Figure 1: (a) Space-time elements and (b) test function.

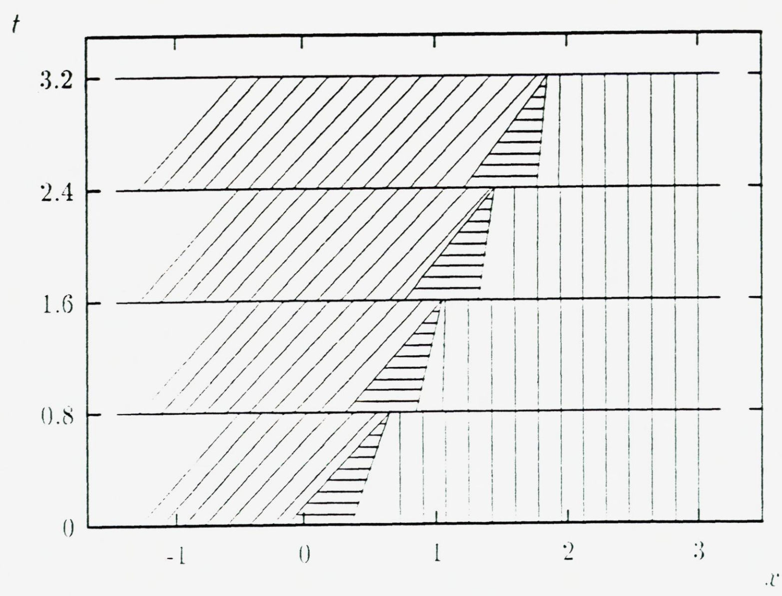

Figure 2: Space-time elements at successive time steps for the example in Figure 3. Shock regions R_s, are marked by horizontal lines.

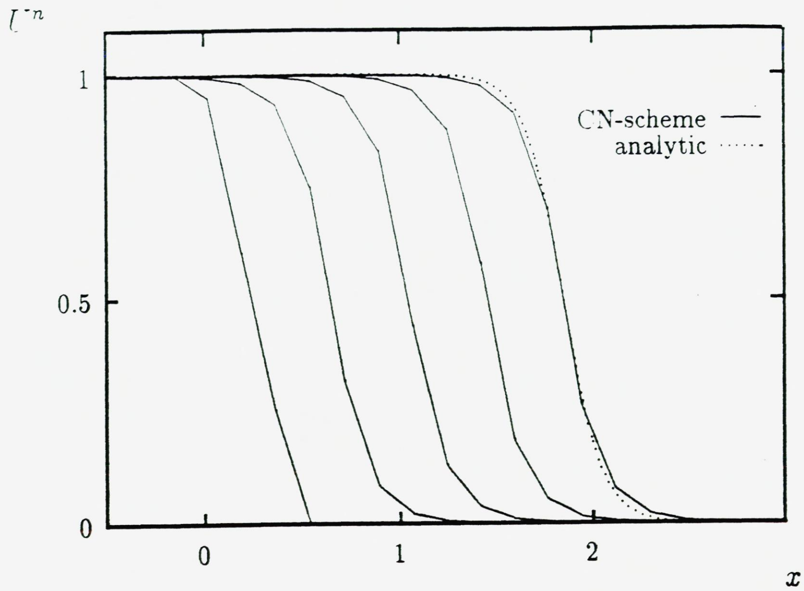

Figure 3: Solution at successive time steps, $n = 0, 1, ..., 4$; $\Delta x = 0.175$, $\Delta t = 0.8$, $\Delta \boldsymbol{x}_g = 0.0175$, $\Delta t_g = 0.0087$.

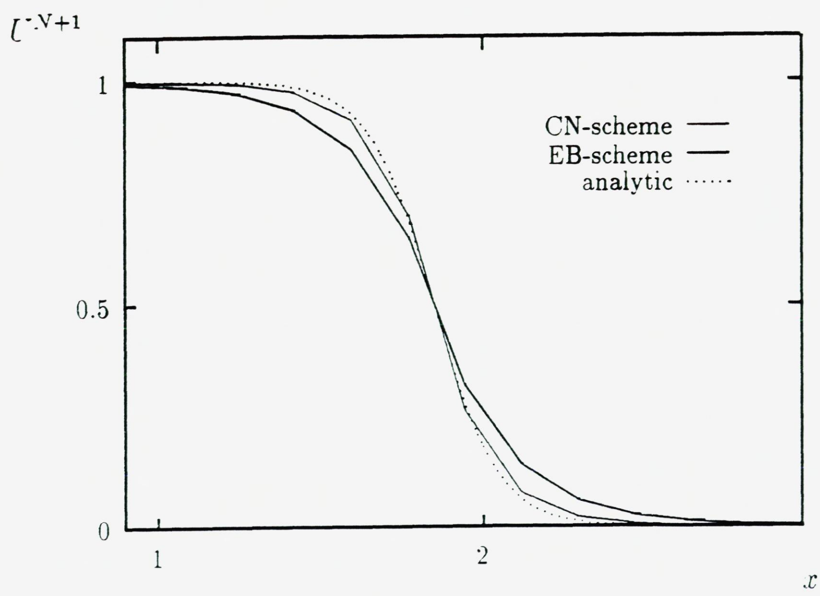

Figure 4: Front region at $t^{N+1} = 3.2$: $\Delta x = 0.175$, $\Delta t = 0.8$, $\Delta x_g = 0.0175$, $\Delta t_g = 0.0087$.

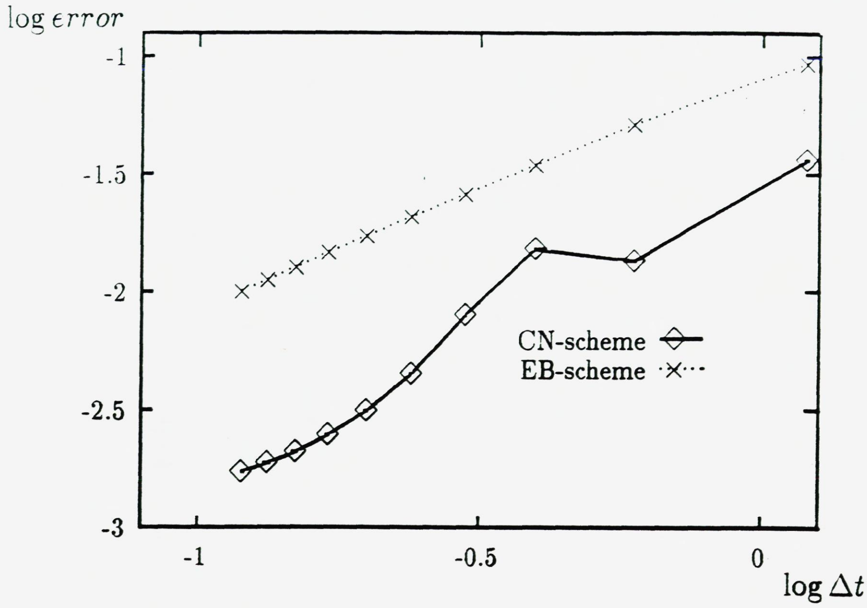

Figure 5: Logarithm of the $L_2 - error$ versus logarithm of Δt; $t^{N+1} = 2.4$, $\Delta x = 0.0044$, $\Delta x_g = 0.0022$, $\Delta t_g = 0.0011$.

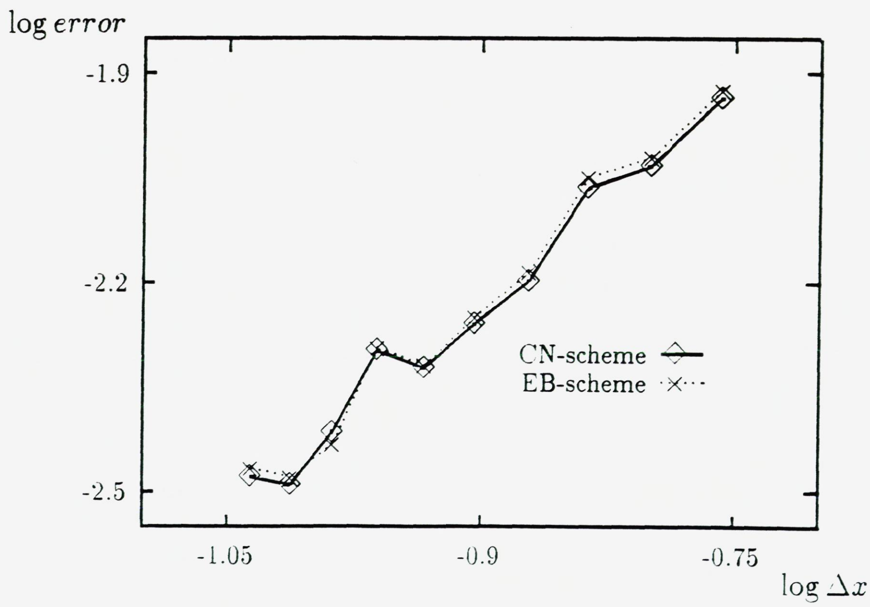

Figure 6: Logarithm of the $L_2 - error$ versus logarithm of Δx; $t^{N+1} = 2.4$, $\Delta t = 0.01$, $\Delta x_g \sim 0.01$, $\Delta t_g \sim 0.005$.

Depotbiblioteket
78sd 20 247